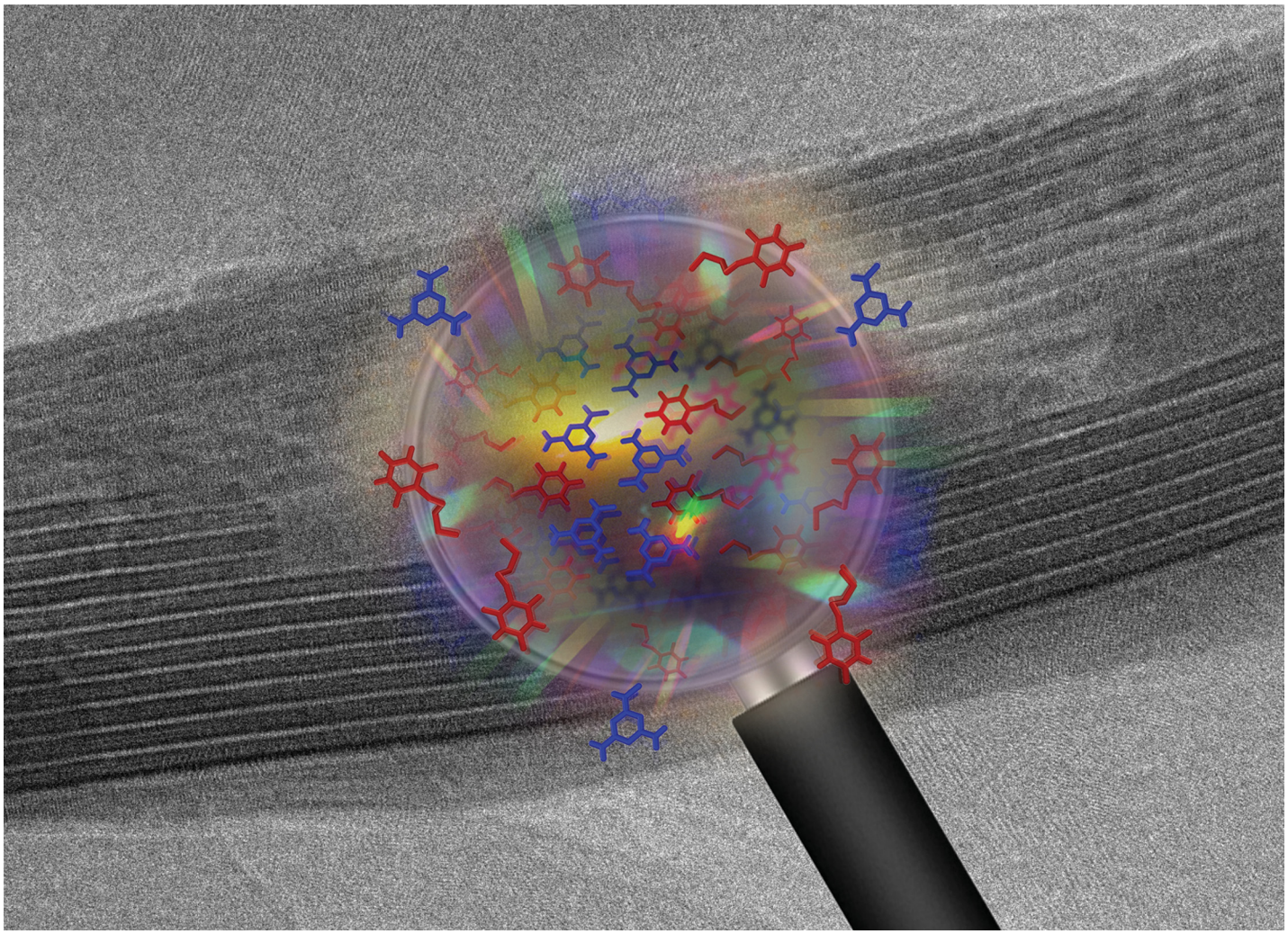

Showcasing research from the laboratories of Sergey N. Semenov in Weizmann Institute of Science and Ekaterina V. Skorb in ITMO University

Altering the structures of 3D supramolecular assemblies from melamine and cyanuric acid derivatives in water

The illustration shows a molecular resolution TEM image of the layered structure formed from melamine and cyanuric acid derivatives, which are artistically depicted in the center. This work highlights the sensitivity of self-assembly in water to the balance between various noncovalent interactions.

As featured in:

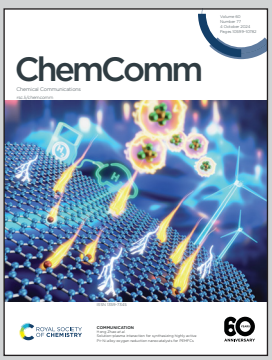

See Sergey N. Semenov, Ekaterina V. Skorb *et al.*, *Chem. Commun.*, 2024, **60**, 10680.

ROYAL SOCIETY OF CHEMISTRY

rsc.li/chemcomm

Registered charity number: 207890

ChemComm

COMMUNICATION

View Article Online
View Journal | View Issue

Cite this: *Chem. Commun.*, 2024, **60**, 10680

Received 10th June 2024,
Accepted 8th August 2024

DOI: 10.1039/d4cc02817a

rsc.li/chemcomm

Altering the structures of 3D supramolecular assemblies from melamine and cyanuric acid derivatives in water†

Nikita Orekhov,[ad] Nina Bukhtiiarova,[ab] Zlata A. Brushevich,[a] Anton A. Muravev,[a] Elad Nadav,[c] Yael Tsarfati,[b] Anna Kossoy,[c] Isai Feldman,[c] Anastasia Zelenina,[d] Anna A. Rubekina,[e] Sergey N. Semenov *[b] and Ekaterina V. Skorb *[a]

Herein, we obtained two supramolecular assemblies with layered structures from melamine, *N*-methylmelamine, and hexynyl-cyanuric acid in water. By combination of X-ray diffraction, electron microscopy, and molecular dynamics studies, we found that introducing one methyl group in melamine alters the arrangement of the layers in these structures.

Supramolecular structures formed through non-covalent interactions have much potential for applications such as responsive soft materials,[1] biomedical materials, membranes,[2] and catalysts.[3] Among the many molecular scaffolds that are used to construct supramolecular structures, the derivatives of melamine and cyanuric acid were one of the first to be employed and currently remain among the most frequently used.[4–9] These derivatives provide multiple triple hydrogen bonds with a 120° angle between them. These hydrogen bonds result in well-defined structural motifs such as hexad rosettes, linear, and zig-zag tapes.[10–12] Not surprisingly, most of the original studies on the self-assembly of these molecules were conducted in non-aqueous solvents in which hydrogen-bonding interactions play a dominant role in defining the final structures.[11,13,14] Nevertheless, the potential application of these structures as biocompatible soft materials and even their potential role in the origin of life assume that they will operate in water, where π–π stacking and other noncovalent interactions compete with hydrogen bonding.[15,16] Pioneering studies by Hud and coworkers on the self-assembly of these molecules in water focused on 1D fibers assembled from the 0D rosette motif. Here the contributions of hydrogen bonding, π–π stacking, and other interactions in the formation of the final structure are somewhat modular and controllable.[17–19] However, assembly in rosette motifs often requires highly engineered molecules with bulky substituents. Melamine and cyanuric acid with small aliphatic substituents are likely to be arranged in 1D tape motifs. Predicting the final structures formed from these motifs in water remains challenging because they are likely to further assemble into 2D sheets and finally into 3D materials with varying degrees of order. Moreover, experimental studies using these assemblies are often hampered by the difficulty in characterizing the final 3D structures, which are usually not crystalline enough for single-crystal X-ray diffraction and are more challenging for electron microscopy characterization than are 1D fibers. Notable examples of non-fibrous assemblies in water include lipid bilayers from melamine and cyanuric acid derivatives containing long aliphatic chains.[20–22]

Here, we characterized two 3D supramolecular structures formed from hexynyl-cyanuric acid (HCA) and melamine (M) or *N*-methyl melamine (MM) by combining high-resolution transmission electron microscopy (TEM), powder X-ray diffraction (XRD), and molecular dynamics (MD) simulations. Interestingly, the small change in molecular building blocks originating from methyl substituents in the melamine altered the final structures.

We used HCA, M, and MM as building blocks for the supramolecular structures in this study (Fig. 1). HCA was chosen for two reasons: (i) it can form two triple hydrogen bonds at 120°, and therefore, it can participate in rosette and tape motifs; (ii) its alkyne group can facilitate further surface modification of the materials by the azide–alkyne click reaction. M and MM were chosen because they are the simplest complementary blocks for HCA. However, methylation introduces an important difference into the properties of these molecules: if M can form 3 strong triple hydrogens, MM can form only 2 strong

[a] *Infochemistry Scientific Center, ITMO University, Saint Petersburg, Russia. E-mail: skorb@itmo.ru*
[b] *Department of Molecular Chemistry and Materials Science, Weizmann Institute of Science, Rehovot, Israel. E-mail: sergey.semenov@weizmann.ac.il*
[c] *Department of Chemical Research Support, Weizmann Institute of Science, Rehovot, Israel*
[d] *Moscow Center for Advanced Studies, Moscow, Russia*
[e] *Lomonosov Moscow State University, Moscow, Russia*

† Electronic supplementary information (ESI) available: Synthetic, analytical, and computational protocols, Fig. S1–S11. See DOI: https://doi.org/10.1039/d4cc02817a

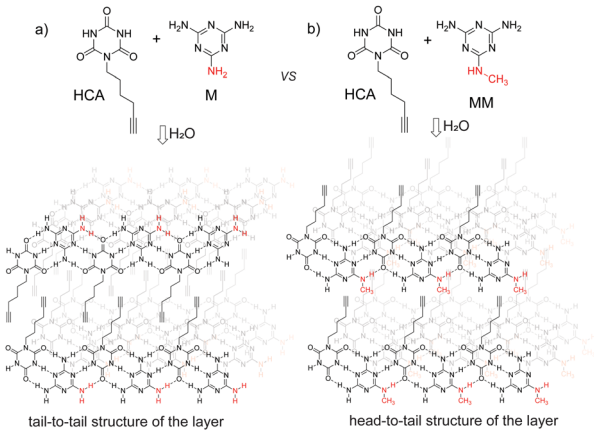

Fig. 1 Layered structures formed by self-assembly of hexynil cyanuric acid with (a) melamine and (b) *N*-methylmelamine.

hydrogen bonds, and a third bond will be disrupted by the methyl group.

We synthetized HCA by reacting the mesylate of hex-5-yn-1-ol with cyanuric acid in the presence of DBU.[23] The supramolecular materials (Fig. 1) were initially obtained by mixing equimolar amounts of aqueous solutions of HCA (10 mM) and M (10 mM) or MM (10 mM) and then filtering the formed precipitates. Experimentally, the acceptable range of the concentrations of the reacting solutions is from 1–10 mM. At lower concentrations, a precipitate did not form, and higher concentrations are not accessible because of the solubility of HCA. The materials formed in this way have low crystallinity according to powder XRD (Fig. S1, ESI†). More crystalline materials, which were used for structural studies, were obtained by mixing solutions at 80 °C (when precipitation does not occur) and slowly cooling the mixture in a Dewar flask.

The materials obtained by slow cooling showed well-defined XRD patterns (Fig. 2a and b). These patterns pointed towards layered structures; the first peaks can be attributed to a series with 23.85 and 28.36 Å spacing for the M*HCA and MM*HCA structures, correspondingly. From the geometrical considerations, a distance of 28 Å roughly corresponds to the doubled thickness of M*HCA H-bonded tape (~14 Å), whereas a distance of 24 Å might correspond to two M*HCA tapes with intertwined hexynyl tails (Fig. 2c and d). For M*HCA the first peak in the series (d = 23.85 Å) is strong, but for MM*HCA the second peak in the series (d = 14.18 Å) is the strongest; however, the first peak (d = 28.36 Å) is very weak. This relationship between the first and second peaks in the series was retained in patterns obtained from samples in capillaries (Fig. S2, ESI†) and in measurements with transmission instead of reflection geometry (Fig. S3, ESI†); therefore, the effects due to the preferable orientation of the crystallites were eliminated. In addition, scanning electron microscopy images of the samples used for XRD revealed no preferable orientation of microcrystals (Fig. S4–S8, ESI†), but instead, a sponge-like morphology with no preferential direction. These observations indicate the existence of destructive interference for the reflection corresponding to the first peak in MM*HCA, which would be expected for the arrangement shown in Fig. 2d. In addition, both XRD patterns have strong peaks at around 3.3 Å (3.31 Å for M*HCA and 3.36 Å for MM*HCA), which is typical for π–π stacked layers in melamine cyanurate.[24] Nevertheless, the quality of the XRDs was insufficient for complete indexing and structural determination. Therefore, we decided to use it in combination with high-resolution TEM and MD simulations to confirm the major structural motifs in these materials.

In the TEM studies, we used two protocols for sample preparation: with and without cryo-drying. The best results for M*HCA were obtained without cryo-drying. The images showed flat crystallites with a layered structure (Fig. 3a, see also Fig. S9 and S10, ESI†). The side view of a crystallite clearly showed layers with spacing of about 23.9 Å, which is in excellent correspondence with XRD. The top view of a crystallite showed a spacing of 3.3 Å, again an excellent correspondence with XRD. All together, TEM resembled the structure shown in Fig. 1, with double-layers of M*HCA in which the hexynyl tails point towards each other.

For MM*HCA, the quality of the TEM images was generally lower than that of M*HCA. Nevertheless, the image capturing the side view of a crystallite (Fig. 3b) showed a spacing of 14.5 Å, which is a good agreement with 14.03 Å for the strongest reflection in XRD. FFT analysis of the top view of the crystallite (Fig. 3c) revealed a spacing of 3.7 Å, which is in reasonable agreement with 3.4 Å observed in XRD. Overall, the XRD and TEM studies pointed towards layered structure shown in Fig. 1.

To further confirm the proposed structures of M*HCA and MM*HCA, we constructed their models using MD (Fig. 4a and b).[25,26] The models confirmed the periodicity observed in XRD and TEM as well as gave a good agreement between experimental and calculated XRD patterns (Fig. 4c and d). To better understand the differences between the two structures, we compared the potential energies of interatomic interactions per pair of molecules E for the tail-to-tail and head-to-tail arrangements of layers made of M*HCA and MM*HCA (Fig. 4e). The figure shows that the M*HCA tail-to-tail

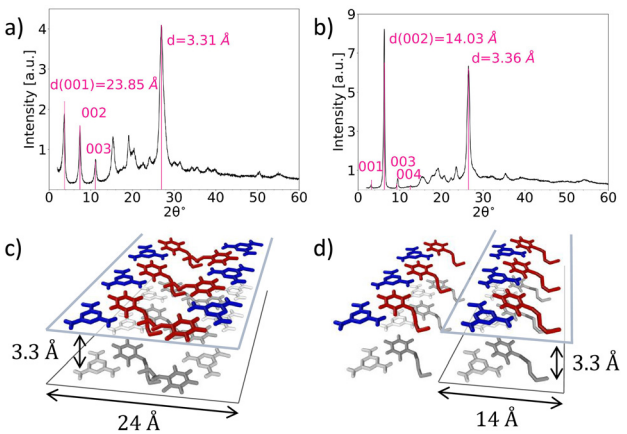

Fig. 2 XRD patterns of M*HCA (a) and MM*HCA (b) as well as estimation of characteristic periods for tail-to-tail (c) and head-to-tail (d) arrangements.

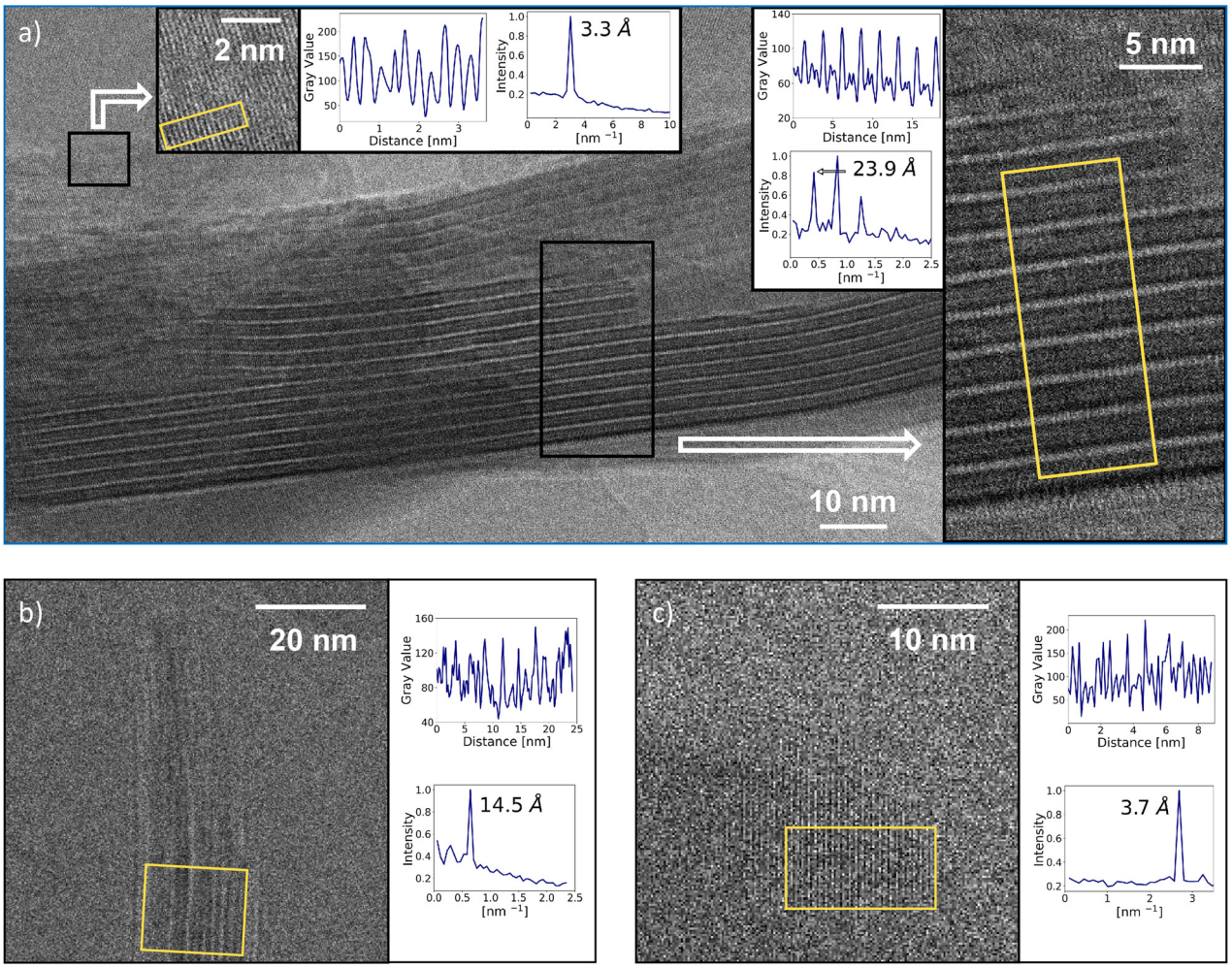

Fig. 3 (a) TEM images of M*HCA. The profiles were taken along long axes and averaging was performed along the short axes of the yellow rectangles. The inserts show the resulting profiles, their FFT, and the characteristic periodicity. (b) and (c) Cryo-TEM images of MM*HCA. The analysis was performed similarly to (a).

arrangement is favored over the head-to-tail arrangement by about 10 kcal mol^{-1}. For MM*HCA, these two arrangements are energetically approximately equivalent. Thus, for M*HCA, one of the reasons for its tail-to-tail arrangement is its higher thermodynamic stability, compared with the head-to-tail arrangement. However, during the growth of these structures, the kinetic factors are more likely to define the final arrangements than are the thermodynamic factors. Therefore, we performed two 500 ns-long MD simulations of M*HCA and MM*HCA surface growth from the water solution. For M*HCA crystal, we observe the orientation of molecules in newly formed layers resulting in the tail-to-tail arrangement that facilitates M–M hydrogen bonding (Fig. S11a, ESI†), while for MM*HCA these layers are more amorphous (Fig. S11b, ESI†). This amorphous nature can be attributed to the shorter timescale of MD simulations in comparison with real experiments, which does not provide enough time for molecules to arrange properly.

In summary, we characterized two layered supramolecular structures assembled in water from melamine and cyanuric acid derivatives. The layers in both structure consist of H-bonded tapes stacked by π–π interactions. Interestingly, these layers are arranged differently for the assemblies, differing by only one methyl group in the melamine component. M forms the structure with a tail-to tail arrangement and the bilayer is the major repeating motif, whereas MM forms the structure with a head-to tail arrangement and the monolayer is the major repeating motif. The balance between H-bonding and van der Waals interactions likely plays a critical role in this difference.[3,15] M favors H-bonding, an interaction that holds bilayers in the tail-to tail arrangement; however, the methyl group hampers these interactions for the MM-based assembly to the extent where they become comparable to the van der Waals interactions between MM and hexynyl tails of HCA. In the context of supramolecular chemistry, this work highlights the fact that water is a unique solvent in which the balance between all types of non-covalent interactions is important in defining the final structure. Therefore, highly ordered structures can be obtained from very simple building blocks such as

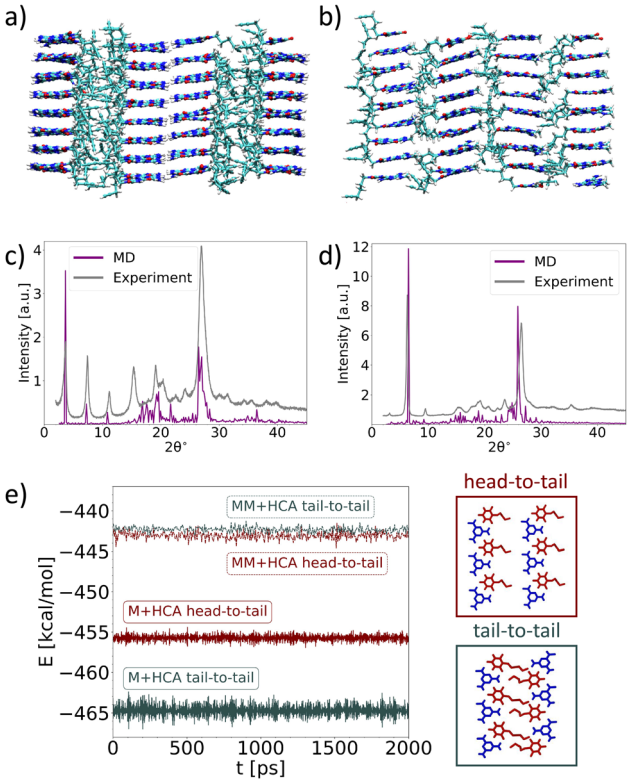

Fig. 4 Atomistic structures of (a) M*HCA and (b) MM*HCA obtained in MD simulations at T = 300 K. (c) and (d) Comparison of XRDs calculated from MD simulations with experimental XRDs. (e) Time evolution of the normalized potential energy of M*HCA (solid lines) and MM*HCA (dashed lines) systems with molecules arranged into two possible configurations: "head-to-tail" (red lines) and "tail-to-tail" (black lines).

M, MM, and HCA in water. In the context of materials science, the reversibility of the assembly-disassembly of these structures upon heating in water and in the presence of the "clickable" alkyne groups opens the possibility to use these compounds as scaffolds for dynamic functional materials.

S. N. S. and E. V. S. supervised the research. S. N. S., E. V. S., N. O. and N. B. designed experiments. N. B., Z. A. B, and A. A. M. synthesized starting materials. N. B. synthesized M*HCA and MM*HCA. N. O., A. Z. and A. A. R. performed MD simulations. N. E. and Y. T. performed and analyzed TEM measurements. A. K. performed and analyzed SEM measurements. I.F. performed and analyzed XRD measurements. E. V. S., N. O., A. Z. and S. N. S. wrote the manuscript.

Authors thank Alexandr Mityaev and Alexander Tsirlin for helpful discussions. Authors acknowledge RSF grant no. 24-13-00355 for the support. We thank Priority 2030 for infrastructural support. A. A. R. acknowledges support from the Fund of Theoretical Physics and Mathematics Development "BASIS" No. 20-2-10-6-1.

Data availability

The data supporting this article have been included as part of the ESI.†

Conflicts of interest

There are no conflicts to declare.

Notes and references

1 A. J. Savyasachi, O. Kotova, S. Shanmugaraju, S. J. Bradberry, G. M. Ó'Máille and T. Gunnlaugsson, *Chem*, 2017, **3**, 764–811.
2 P. Meng, A. Brock, Y. Xu, C. Han, S. Chen, C. Yan, J. McMurtrie and J. Xu, *J. Am. Chem. Soc.*, 2020, **142**, 479–486.
3 E. Krieg, M. M. Bastings, P. Besenius and B. Rybtchinski, *Chem. Rev.*, 2016, **116**, 2414–2477.
4 S. Yagai, M. Usui, T. Seki, H. Murayama, Y. Kikkawa, S. Uemura, T. Karatsu, A. Kitamura, A. Asano and S. Seki, *J. Am. Chem. Soc.*, 2012, **134**, 7983–7994.
5 V. V. Korolkov, M. Baldoni, K. Watanabe, T. Taniguchi, E. Besley and P. H. Beton, *Nat. Chem.*, 2017, **9**, 1191–1197.
6 C. T. Seto and G. M. Whitesides, *J. Am. Chem. Soc.*, 1990, **112**, 6409–6411.
7 G. M. Whitesides, J. P. Mathias and C. T. Seto, *Science*, 1991, **254**, 1312–1319.
8 J. P. Mathias, E. E. Simanek, C. T. Seto and G. M. Whitesides, *Angew. Chem., Int. Ed. Engl.*, 1993, **32**, 1766–1769.
9 L. J. Prins, F. De Jong, P. Timmerman and D. N. Reinhoudt, *Nature*, 2000, **408**, 181–184.
10 A. Alenaizan, C. H. Borca, S. C. Karunakaran, A. K. Kendall, G. Stubbs, G. B. Schuster, C. D. Sherrill and N. V. Hud, *J. Am. Chem. Soc.*, 2021, **143**, 6079–6094.
11 J. A. Zerkowski, C. T. Seto, D. A. Wierda and G. M. Whitesides, *J. Am. Chem. Soc.*, 1990, **112**, 9025–9026.
12 A. G. Bielejewska, C. E. Marjo, L. J. Prins, P. Timmerman, F. de Jong and D. N. Reinhoudt, *J. Am. Chem. Soc.*, 2001, **123**, 7518–7533.
13 D. N. Chin, D. M. Gordon and G. M. Whitesides, *J. Am. Chem. Soc.*, 1994, **116**, 12033–12044.
14 M. Mammen, E. E. Simanek and G. M. Whitesides, *J. Am. Chem. Soc.*, 1996, **118**, 12614–12623.
15 C. M. Leenders, M. B. Baker, I. A. Pijpers, R. P. Lafleur, L. Albertazzi, A. R. Palmans and E. W. Meijer, *Soft Matter*, 2016, **12**, 2887–2893.
16 W. Zhang and Y. Chen, *Front. Chem.*, 2023, **11**, 1346014.
17 B. J. Cafferty, I. Gallego, M. C. Chen, K. I. Farley, R. Eritja and N. V. Hud, *J. Am. Chem. Soc.*, 2013, **135**, 2447–2450.
18 B. J. Cafferty, R. R. Avirah, G. B. Schuster and N. V. Hud, *Chem. Sci.*, 2014, **5**, 4681–4686.
19 B. J. Cafferty, D. M. Fialho, J. Khanam, R. Krishnamurthy and N. V. Hud, *Nat. Commun.*, 2016, **7**, 11328.
20 T. Kawasaki, M. Tokuhiro, N. Kimizuka and T. Kunitake, *J. Am. Chem. Soc.*, 2001, **123**, 6792–6800.
21 N. Kimizuka, T. Kawasaki, K. Hirata and T. Kunitake, *J. Am. Chem. Soc.*, 1998, **120**, 4094–4104.
22 N. Kimizuka, T. Kawasaki and T. Kunitake, *J. Am. Chem. Soc.*, 1993, **115**, 4387–4388.
23 Y. Wang, P. J. Santos, J. M. Kubiak, X. Guo, M. S. Lee and R. J. Macfarlane, *J. Am. Chem. Soc.*, 2019, **141**, 13234–13243.
24 T. J. Prior, J. A. Armstrong, D. M. Benoit and K. L. Marshall, *CrystEngComm*, 2013, **15**, 5838–5843.
25 T. A. Aliev, A. A. Timralieva, T. A. Kurakina, K. E. Katsuba, Y. A. Egorycheva, M. V. Dubovichenko, M. A. Kutyrev, V. V. Shilovskikh, N. Orekhov, N. Kondratyuk, S. N. Semenov, D. M. Kolpashchikov and E. V. Skorb, *Nano Select*, 2022, **3**, 1526–1536.
26 N. Orekhov, N. Kondratyuk, M. Logunov, A. Timralieva, V. Shilovskikh and E. V. Skorb, *Cryst. Growth Des.*, 2021, **21**, 1984–1992.